Journal of Power Sources 247 (2014) 503–516

Contents lists available at ScienceDirect

Journal of Power Sources

journal homepage: www.elsevier.com/locate/jpowsour

Characterizing and modeling mechanical properties and onset of short circuit for three types of lithium-ion pouch cells

Elham Sahraei [a,*], Joseph Meier [a], Tomasz Wierzbicki [b,1]

[a] Impact and Crashworthiness Lab, Massachusetts Institute of Technology, 77 Massachusetts Ave, Room 5-218B, Cambridge, MA 02139, USA
[b] Impact and Crashworthiness Lab, Massachusetts Institute of Technology, 77 Massachusetts Ave, Room 5-218A, Cambridge, MA 02139, USA

HIGHLIGHTS

- Detecting onset of short circuit due to mechanical loads and deformations.
- Developing homogenized material models for the interiors of three pouch cells.
- Finite element modeling of crush behavior of the cells.

ARTICLE INFO

Article history:
Received 3 April 2013
Received in revised form
18 July 2013
Accepted 12 August 2013
Available online 27 August 2013

Keywords:
Pouch cell
Lithium-ion
Short circuit
Mechanical abuse
Finite element modeling

ABSTRACT

Three types of lithium ion pouch cells ranging from small consumer electric cells with $LiCoO_2$ cathode to large (electric vehicle size) cells with nanophosphate chemistry were tested under several local and global compression scenarios, including compression between two flat plates and local indentation with a flat cylindrical punch, a conical punch, and three hemispherical punches. Load, displacement, temperature, and voltage were recorded in all tests. The punch displacements were stopped when a drop in force and voltage of the cell, as well as a rise in temperature indicated a short circuit in the cell. Finite element models were developed for each cell type. Two tests were used for calibration of the constitutive properties of each type of cell, and the remaining tests served for the validation of the computational model. The models successfully predicted the load displacement relation and contour of deformations in the cells. Additionally, the models closely predict the force and punch displacement corresponding to the onset of short circuit in the cell. The current results are building confidence in robustness and accuracy of the present calibration and modeling approach.

1. Introduction

Lithium-ion batteries are used in many transportation applications like Plug-in Hybrid and Electric Vehicles (PhEV, EV), electric buses, and airplanes. The difference between these applications of the lithium-ion batteries and the ones in consumer electronics is that a battery in a moving vehicle is constantly operating under a variety of speeds and accelerations. A moving battery is exposed to local forces and deformations that in extreme cases, such as in a vehicle crash, can result in local damage of the cell. Excessive damage can ultimately cause an internal short circuit in the battery cell. This can happen even if the exterior casing of the cell does not fail or fracture. A short circuit in a battery pack can result in smoke generation or combustion of the battery pack, as seen in cases of the Chevrolet Volt, and Boeing 787 Dreamliner [1,2].

The need to better understand the behavior of batteries under mechanical loading and the conditions that lead to an electric short circuit has motivated this research. Internal short circuit in lithium-ion batteries has been studied in the past experimentally using nail penetration or pinch tests [3–5]. The thermal properties and models of lithium-ion cells under thermal abuse conditions have also been subject of several studies [6–9]. However, papers on mechanical properties and mechanical conditions that lead to a short circuit are limited. Mechanical properties of the cells or cell components during intercalation and normal use of batteries were reported in literature [10–14]. The only publications known to the authors on mechanical properties leading to short circuit in a cell are by Sahraei et al., Wierzbicki and Sahraei, and Greve and Fehrenbach [15–18].

Sahraei et al., 2012 [17] studied the mechanical properties of a small pouch cell in several loading conditions by using an extensive

* Corresponding author. Tel.: +1 6173245025.
E-mail addresses: elhams@mit.edu (E. Sahraei), joemeier@mit.edu (J. Meier), wierz@mit.edu (T. Wierzbicki).
[1] Tel.: +1 617 253 2104; fax: +1 617 253 8689.

0378-7753/$ – see front matter © 2013 Elsevier B.V. All rights reserved.
http://dx.doi.org/10.1016/j.jpowsour.2013.08.056

Table 1
Specifications of the three types of cells.

	Small pouch cell	Medium pouch cell	Large pouch cell
Nominal capacity	740 mAh	3.2 Ah	19.5 Ah
Nominal voltage	3.7 V	3.7 V	3.3 V
Thickness	5.35 mm	8.2 mm	7.25 mm
Width	34 mm	43.5 mm	160 mm
Length	59.5 mm	129.5 mm	227 mm
Weight	19 g	85 g	496 g
Chemistry	$LiCoO_2$	$LiMnNiCoO_2$	Nanophosphate

experimental program. A numerical model was developed to predict the properties observed during the tests. In a second study [16], the same team calibrated mechanical properties of an 18650 cylindrical cell, and developed finite element models that predicted not only the load displacement properties of the cells, but also the deformation levels that lead to internal short circuit. Mechanical properties of cylindrical cells and the related numerical models for a medium size cylindrical cell were reported by Greve and Fehrenbach 2012 [18]. They also proposed a criterion for detecting short circuit in the cell. However, the same tests were used for calibration and validation. Wierzbicki and Sahraei 2013 proposed an analytical procedure to extract homogenized properties of jellyroll from compression tests of the entire cylindrical cell between two flat plates. The proposed analytical method was validated by using the calibrated material properties in a finite element model of the cell, which predicted the test results with a very good accuracy.

The current study complements the work listed above by providing the test results on three types of pouch cells. The tests were specifically designed to report on the mechanical conditions leading to development of an electric short circuit in those cells. Thus, the objective of this paper is to demonstrate that the current homogenous and isotropic constitutive model of the jellyroll is suitable for a range of battery chemistries, cell sizes, and loading conditions. Five types of punches were used for local indentation of the cell. Load, displacement, temperature, and voltage were measured through all tests, to accurately detect onset of short circuit. In the next step, analytical procedures were laid out to extract material and mechanical properties of the cell. Then, a finite element model of each cell was developed and the calibrated material properties were entered. The results accurately predicted the load, displacement, and deformation profile of the cell as well as internal electric short circuit due to deformation.

2. Description of experiments and test results

Three types of lithium ion cells were used for this research, a small, a medium, and a large pouch cell. Properties of these cells are presented in Table 1. This includes a dimension range of 59–227 mm in length, and nominal capacities of 740 mAh to 19.5 Ah. There are also three different chemistries involved, $LiCoO_2$, $LiMnNiCoO_2$, and Nanophosphate. The cell manufacturers were requested to discharge the cells to 10% or less State Of Charge (SOC) to prevent extreme reactions during the indentation tests. Table 2 provides a summary of tests performed on these cells.

Table 2
Tests performed on the three cell types.

Cell type	Tests performed
Small cell	a. Indentation with a small, medium, and large hemispherical punches and a 90-degree conical punch.
Medium cell	a. Flat compression between two plates b. Indentation testing using a small, medium, and large hemispherical punches and a 90-degree conical punch.
Large cell	a. Indentation testing using small, medium, and large hemispherical punches, a flat cylindrical punch, and a 90-degree conical punch.

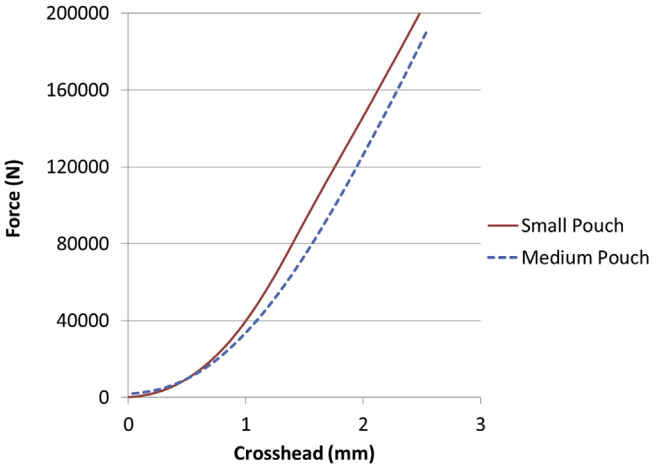

Fig. 1. Medium and small pouch cells, flat compression test results.

In all cases, the pouch cells were tested using a 200 kN MTS compression/tension test machine. Load cells with a maximum range of 10 kN and 200 kN were available for the tests, and appropriately selected based on anticipated maximum test load in each case. A flat compression test was the main type of test to calibrate compression properties of the cells. Such a test was already performed on the small pouch cell as reported in Sahraei et al., 2012 [17]. For this research the medium pouch cell was also tested in the compression mode between two flat platens. This test could not be conducted on large cells because the cell size was larger than the test machine platens and the force developed would far exceed the limit of the available equipment.

Tests were conducted using a fixed displacement rate of 1 mm per minute (quasi-static), and they were run until either the maximum load cell rating was reached, or the cell showed evidence of an internal short circuit. The following parameters were measured and recorded at 1-s intervals:

- Test machine load and crosshead displacement over time
- Cell voltage over time, measured with a typical voltmeter at the cell terminals
- Cell surface temperature over time, monitored via thermocouple
- Photographs of the cell at the punch site, at a rate of one picture per second

Once short-circuit was achieved, temperature and voltage monitoring continued until those parameters returned to a steady-state condition.

2.1. Compression between two plates

The flat compression tests on small pouch cells were reported by Sahraei et at [17], and the results of those tests were used to calibrate the present model of the small cell, for the sake of completeness, the load-displacement for the small cell is included in Fig. 1. Additionally, a medium pouch cell was placed flat between two 8-inch platens in a test machine with voltage and temperature measurement devices attached as discussed in the previous section. The cell maintained stable voltage and temperature, indicating no short circuit during this test. The test was

stopped when the maximum device load limit of 190 kN was reached. A flat compression test of large cells could not be performed with the available equipment, because of size and force limitations of the in-house equipment. Instead, a flat cylindrical punch test (diameter 25.31 mm) was performed on the large cells, see Fig. 2.

In the case of the flat cylindrical punch (large cell only), deformation was localized to the small area adjacent to the punch outer radius. With increase in deflection, it appeared that the sharp edges of the punch surface cut the cell pouch. The ensuing short circuit is more likely a result of the shear stresses rather than tensile stresses that are more dominant for round punches. During more recent tests performed in collaboration with EMI Fraunhofer Institute [19], a large cell was compressed between two flat plates up to 500 kN and still showed no loss in capacity when discharged and recharged after the test. It can be concluded that uniform flat compression of pouch cells will not lead to electric short circuit. Such a uniform load will never be present in real life accident events. Therefore, the remaining tests were done to simulate more local loads. Still, the flat compression tests provided needed information to calibrate the constitutive equations.

2.2. Indentation of cells with hemispherical and conical punches

A comprehensive test program was conducted to complete the calibration procedure and validate the corresponding models. The three types of cells were indented with a series of punches: three hemispherical and one conical shape. Fig. 3 shows the punches used for this research. The flat cylindrical punch was only used on the large pouch cells, as explained in previous section.

The punches were positioned over the center of the cell lengthwise and widthwise, and a thermocouple was attached to the top surface of the cell with adhesive, approximately one inch from the punch footprint to prevent damage to the device. The thermocouple was not placed on the underside of the battery to prevent heat conduction with the temperature of the test machine steel base plate.

Upon short circuit in any of the indentation tests, observed were a simultaneous drop in force, a drop in voltage, and increase of the temperature (see Appendix A). The small and medium pouch cells also showed an inflation of the pouch, due to formation of gases during short circuit chemical reactions, see Fig. 4a and b. This was more intense for the case of medium pouch cells, suggesting the cells possibly had an SOC larger than 10%. The large cells proved to have an SOC close to zero, and exhibited almost negligible temperature increases and no inflation as a result of the indentations, see Fig. 4c.

Fig. 3. Punch sizes used for local indentation, from left to right is a 90° conical punch, hemispherical punches of diameters12.7 mm, 28.575 mm, and 44.45 mm, and a flat cylindrical punch of 25.31 mm.

For all three types of cells, there was a consistent progressing pattern for the load-displacement curves with different punch sizes, meaning that the peak load at short circuit increased with an increase in punch diameter, see Fig. 5. The large hemispherical punch did not produce short circuit until loads reached over 30 kN, while the peak force at short circuit for a conical punch was less than 0.1% of this load.

Fig. 6 shows the rise in temperature of all cells at points of short circuit. For the small pouch, the temperature rise is about 40–50 °C for conical punch and medium/large hemispherical punches. However, the temperature change in case of small hemispherical punch is about 10 °C. The rise in temperature starts earliest for the conical punch and gets delayed with increase in punch diameter for hemispherical punches. Similar trend of delay in short circuit with an increase of punch diameter is observed for medium and large pouch cells as well. For hemispherical punch indentation of medium cell, a decrease in peak temperature is observed with an increase in punch diameter. Similar decrease in peak temperature is observed for small and large cells, only from medium to large hemispherical punches.

Fig. 7 shows the drop in voltage at points of short circuit for all tests. It can be observed from drop in voltage as well that conical punch created short circuit before all other punches did. Small, medium, and large hemispherical punches create short circuit at later points, respectively. A voltage rebound was observed after initial drop for the conical punch indentation of the medium cell, and then the voltage gradually decreased to zero over a period of 600 s.

Graphs of peak load and deformation depth at short circuit versus different punch diameters for all three cells are shown in Fig. 8. It is interesting to note that peak load at short circuit is almost linearly increasing with an increase in punch diameter.

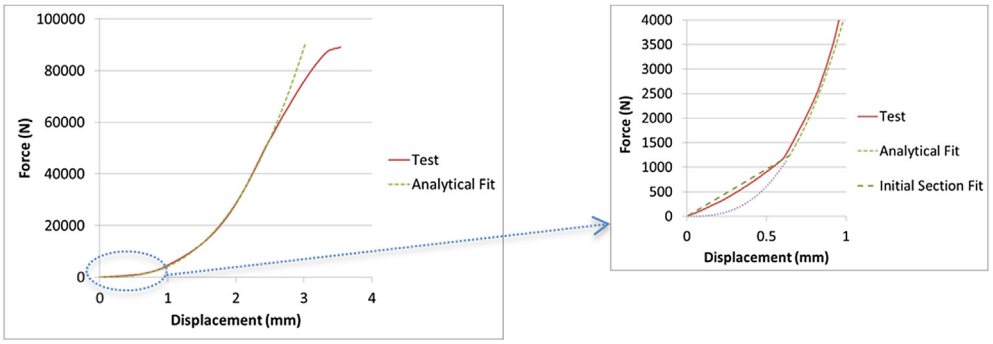

Fig. 2. Flat cylindrical punch indentation of large pouch cell. The test was fitted by a linear line in initial section, followed by a nonlinear curve at displacements more than 0.6 mm. The purple dots show the error that the nonlinear fit could introduce if the whole test would have been fitted with the nonlinear term. (For interpretation of the references to color in this figure legend, the reader is referred to the web version of this article.)

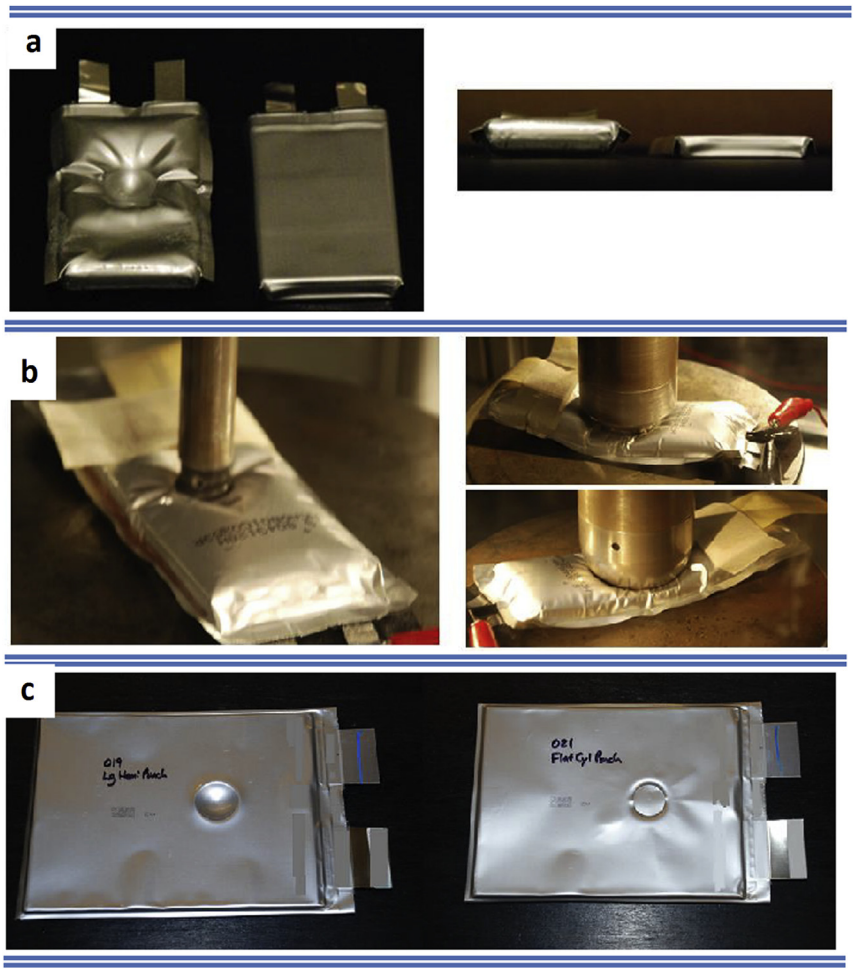

Fig. 4. a) Inflation of the small cell under small hemispherical punch indentation, top and side views, b) Inflation of the medium cell under three hemispherical punch indentations, c) Large cell tested by large hemispherical and flat cylindrical punches.

With the exception of the conical punch experiments, the local deformation that can be tolerated safely by the cells ranges from 3 mm (small and large cells) to 6 mm (medium cell). As expected, the cells develop a short circuit much earlier under the conical punch indentation. The problem is driven by the specific geometry of the cone defined in terms of the central angle and tip radius. The three cells show similar and consistent trends in the two graphs. The above results quantifies the otherwise expected trend that batteries can safely handle intrusion of more blunt objects. No failure was observed for compression between two flat plates, which corresponds to infinite punch radius.

The results of the conical punch indentation of the large cell give an important insight into the mechanics of internal failure and are discussed in this section. For a magnified view of the recorded curves at short circuit of the large cell with a conical punch see Fig. 9. Two separate phases could be observed. In the first phase, at a displacement of about 1.3 mm, a small local peak was observed in the force (highlighted with a circle), while at the same time, a small rise in temperature to about 0.5 °C, and a slight drop in voltage of about 0.05 V was observed. This drop in voltage was not noticeable in full-scale data plots, but could be seen when magnified by a factor of 100, as in Fig. 9. The loading continued, which resulted in three more small peaks in load, subsequent small steps of temperature increase and voltage decrease. In the second phase, at a force of 1200 N, a more distinct drop in force was observed, accompanied by a significant drop in voltage and rise in temperature. These two phases could be distinguished as soft and hard internal short circuits. A hard short circuit is characterized by a concrete connection between anode and cathode, which results in significant drop in voltage and complete discharge of the cell. A soft shot indicates small local contact between electrodes, and slight discharge of the cell, which is not readily detectable in large cells [20]. What is remarkable is that even the soft short circuit is initiated with a local peak in the force and therefore is expected to be predictable from a local mechanical failure in the jellyroll. A soft short circuit due to small mechanical loads may not be distinguished immediately, but may cause delayed reactions in subsequent normal use. This may explain spontaneous thermal runaway and battery fires covered extensively by the media.

3. Constitutive model and calibration procedure

Compressible foam was shown in the literature to describe the basic properties of the jellyroll [15–17]. In the first approximation, the layered structure of the jellyroll is treated as a homogenous and isotropic continuum. The interior of the cell is structurally anisotropic. However, as far as material anisotropy is concerned, except the polymeric separator which is a small portion of the volume of the cell, all other components of the jellyroll (Cu and Al current collectors, graphite and lithium

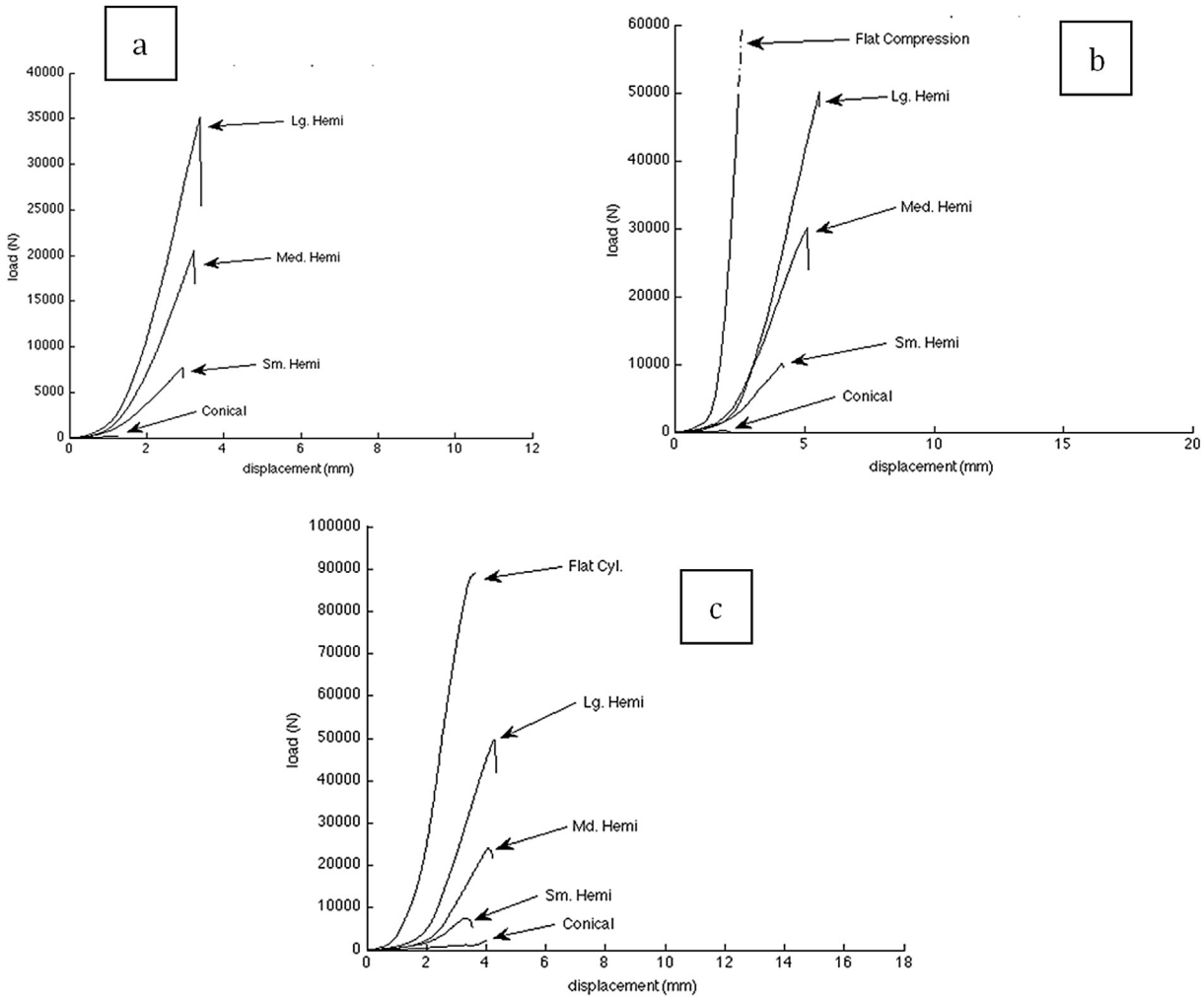

Fig. 5. The load-displacement curves for a) small, b) medium, and c) large pouch cells. Onset of short circuit corresponds with peak load for each test.

metal oxide powders with a binder) are isotropic. Therefore, from the material point of view, the assumption of isotropy is justified.

The effect of the layered nature of the jellyroll was studied experimentally by Sahraei et al. [17]. It was shown that in plane and out of plane compressive properties were very similar. The only difference was due to the buckling strength of the thin Cu and Al foils, sandwiched between much ticker coatings of active material with binder. The response of the jellyroll is characterized by a short range of elastic response, identical in tension and compression. In the elastic range:

$$|\sigma_i| = E\varepsilon_v \quad \nu \sim 0 \tag{1}$$

where σ_i denotes the principal stress, ε_v is the volumetric strain, and E is the effective elastic modulus. The other elasticity parameter, the Poisson ratio, ν is assumed to be small, because of the porous nature of the cell. Equation (1) is valid until the stress reaches the yield stress in compression, Y_c, or the tensile cut off value, Y_t, in tension. Beyond the elastic range, the material flows plastically in a different way in tension and compression. The plastic potential function is defined as:

$$f_i = |\sigma_i| - Y \tag{2}$$

where

$$\begin{aligned} Y &= Y_c + H(\varepsilon_v) \quad \text{for } \sigma_i < 0 (\text{compression}) \\ Y &= Y_t \quad \text{for } \sigma_i > 0 (\text{tension}) \end{aligned} \tag{3}$$

where $H(\varepsilon_v)$ is a hardening function of volumetric strains. Finally, the material unloads elastically with the initial modulus, E. This property requires that the initial modulus be larger than the slope of the load curve at any point, otherwise the unloading path could result in values of $|\sigma_i|$ larger than Y. A conceptual graph of the stress–strain relation is shown in Fig. 10.

The compressive properties for all three types of cells were determined from the tests explained above. The compression tests between two flat plates provided a state of uniaxial strain in the thickness direction for the small and medium pouch cells. The strain in this test is actually the volumetric strain. Therefore, the force-displacement outputs from the small and medium pouch cells, shown in Fig. 1, were used directly to get the compressive stress–strain relationship. A MATLAB curve fitting tool was used to get an analytical power law for each of the constitutive relations. The re-scaling from the force-displacement, (P,w) to the stress–strain relation was done by defining the engineering stress–strain(σ, ε) relation as

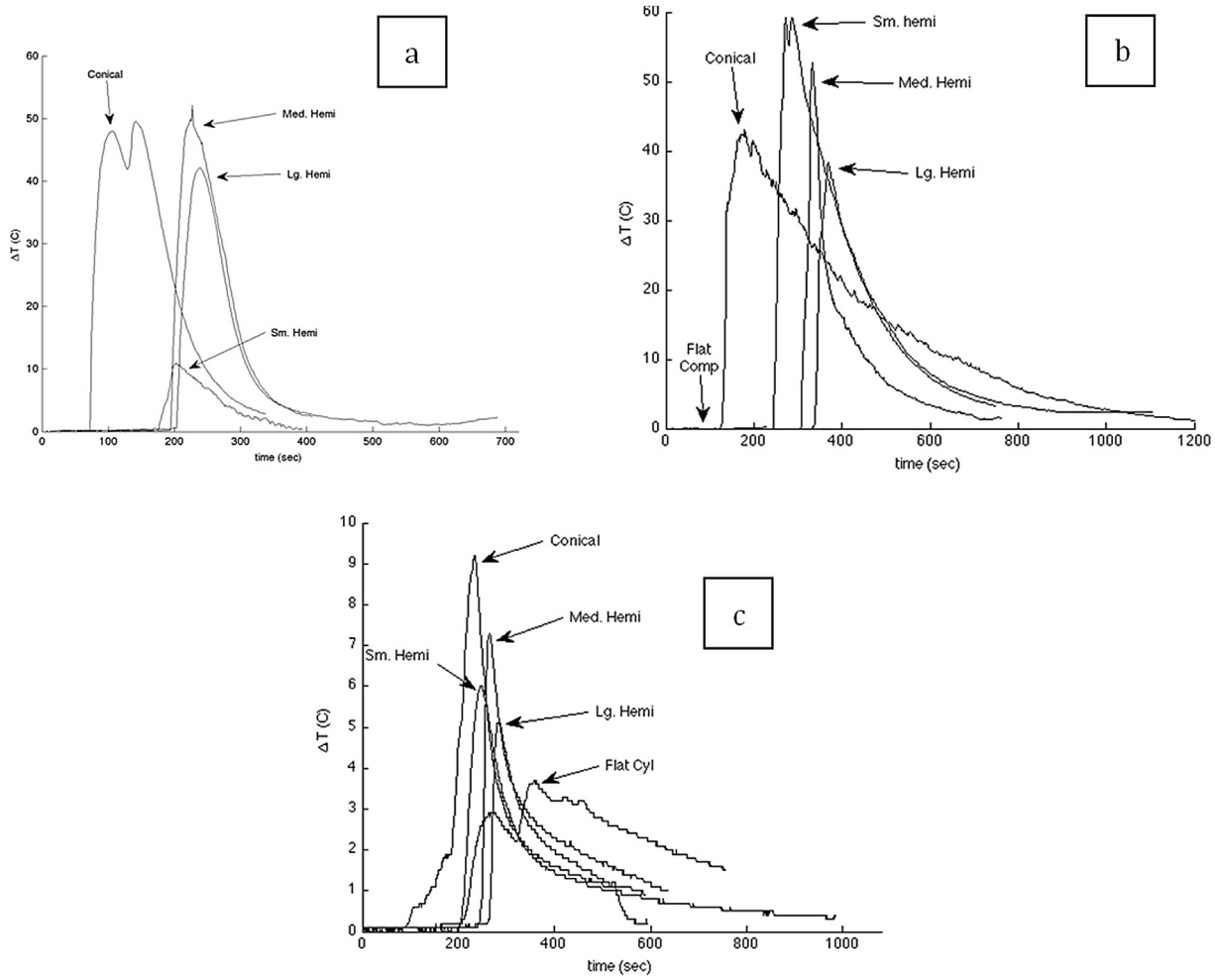

Fig. 6. The change in temperature curves for a) small b) medium, and c) large pouch cells.

$$\sigma = \frac{P}{A_0} \text{ and } \varepsilon = \frac{w}{H} \tag{4}$$

where A_0 is the cross section area of the cell, and H is the cell thickness.

For the large cells, the stress–strain curve was calculated from the flat cylindrical punch test. The details of this method are explained in the next section. To calculate the stress strain curve for the large cylindrical cell from the flat cylindrical punch test, the shape of the deformed section was examined. It was observed that the deformation region included a flat circular area surrounded by a toroid, as shown in Fig. 4c. It is further assumed that due to a low Poisson ratio, the vertical displacement did not induce any radial or angular deformations, and the shear stresses were negligible because of the layers of the cell can slide on top of each other with small friction. Any virtual work in the deformed area would only have components in the vertical direction. Therefore, the plastic work is done only in the vertical direction and the principle of virtual work can be written as:

$$\int_0^R \sigma_1 \dot{\varepsilon}_1 \mathrm{d}v + \int_R^{R+w_0} \sigma_2 \dot{\varepsilon}_2 \mathrm{d}v = P\dot{w}_0 \tag{5}$$

where R is the radius of the punch, σ_1 and $\dot{\varepsilon}_1$ are z components of stress and strain rate in the region under the flat paunch, σ_2 and $\dot{\varepsilon}_2$ are same components in the circumferential toroid area, and w_0 is the depth of indentation. The volume element is $\mathrm{d}v = H(r\mathrm{d}\theta)\mathrm{d}r$. Fig. 11 shows a through-thickness schematic of the deformed area under the flat cylindrical punch. It is assumed that the deformations outside the punch are confined to a quarter of the toroid surface with a radius equal to depth of indentation, w_0.

Considering a uniform strain field through z direction, the engineering strain and strain rate in z direction in the deformed area are:

$$\begin{aligned} &\varepsilon_1 = \tfrac{w_0}{H} \text{ and } \dot{\varepsilon}_1 = \tfrac{\dot{w}_0}{H} \quad 0 < r < R \\ &\varepsilon_2 = \tfrac{w_0(1-\sin\theta)}{H} \text{ and } \dot{\varepsilon}_2 = \tfrac{\dot{w}_0(1-\sin\theta)}{H} \quad R < r < R + w_0,\ 0 < \theta < \pi/2 \end{aligned} \tag{6}$$

where r is the radial coordinate of a deformed element, and can be expressed in terms of the angle θ measured from the center of toroid area as:

$$r = R + w_0(1 - \cos\theta) \tag{7}$$

Guided by the form of the constitutive equation determined for the small and medium pouch cells and 18650 cylindrical cell [15], it

is assumed that the compressive stress–strain relation of the large cell is also of the power type:

$$\sigma = A\varepsilon^n \tag{8}$$

Substituting Equations (6) and (8) in the principal of virtual work, Equation (5), gives:

$$\frac{\dot{w}_0 2\pi A w_0^n}{H^n}\left[\int_0^R r\mathrm{d}r + Rw_0\int_0^{\frac{\pi}{2}}(1-\sin\theta)^{n+1}\sin\theta\mathrm{d}\theta + w_0^2\int_0^{\frac{\pi}{2}}(1-\sin\theta)^{n+1}\sin\theta(1-\cos\theta)\mathrm{d}\theta\right] = P\dot{w}_0 \tag{9}$$

In the above equation, the first integration depends only on the radius of the punch, R, while the second and third integrals depend on the exponent in the constitutive law, n. To make an estimation of contribution of each term in Equation (4), the integrals were evaluated numerically for values of n ranging from 1 to 4, at the indentation depth of $w_0 = 3$ mm. It can be observed from Table 3 that contribution of the 2nd and 3rd term in the right hand side bracket is less than 5% of the contribution of the first term. Therefore, for the purpose of the current paper, those terms can be neglected, and Equation (4) reduces to:

$$\frac{\pi A R^2}{H^n} w_0^n = P \tag{10}$$

where A and n are calculated from an analytical power fit of the measured force displacement relation, as shown in Fig. 2.

By zooming in on the measured load-displacement shown in Fig. 2, one can distinguish a small region of linear behavior, valid for ($0 < w_0 < 0.1$ mm), which can be fitted by a straight line ($P = 1915w_0$), followed by a nonlinear region, best fitted with ($P = 4188w_0^{2.78}$), therefore:

$$\begin{aligned} &P = 1915w_0 \quad \text{for } w_0 < 0.6 \text{ mm} \\ &\text{and } P = 4188w_0^{2.78} \text{for } 0.6 \text{ mm} < w_0 \end{aligned} \tag{11}$$

Comparison of Equations (10) and (11) gives the values for A and n, and the following relation is obtained for the compressive strength of large pouch cell:

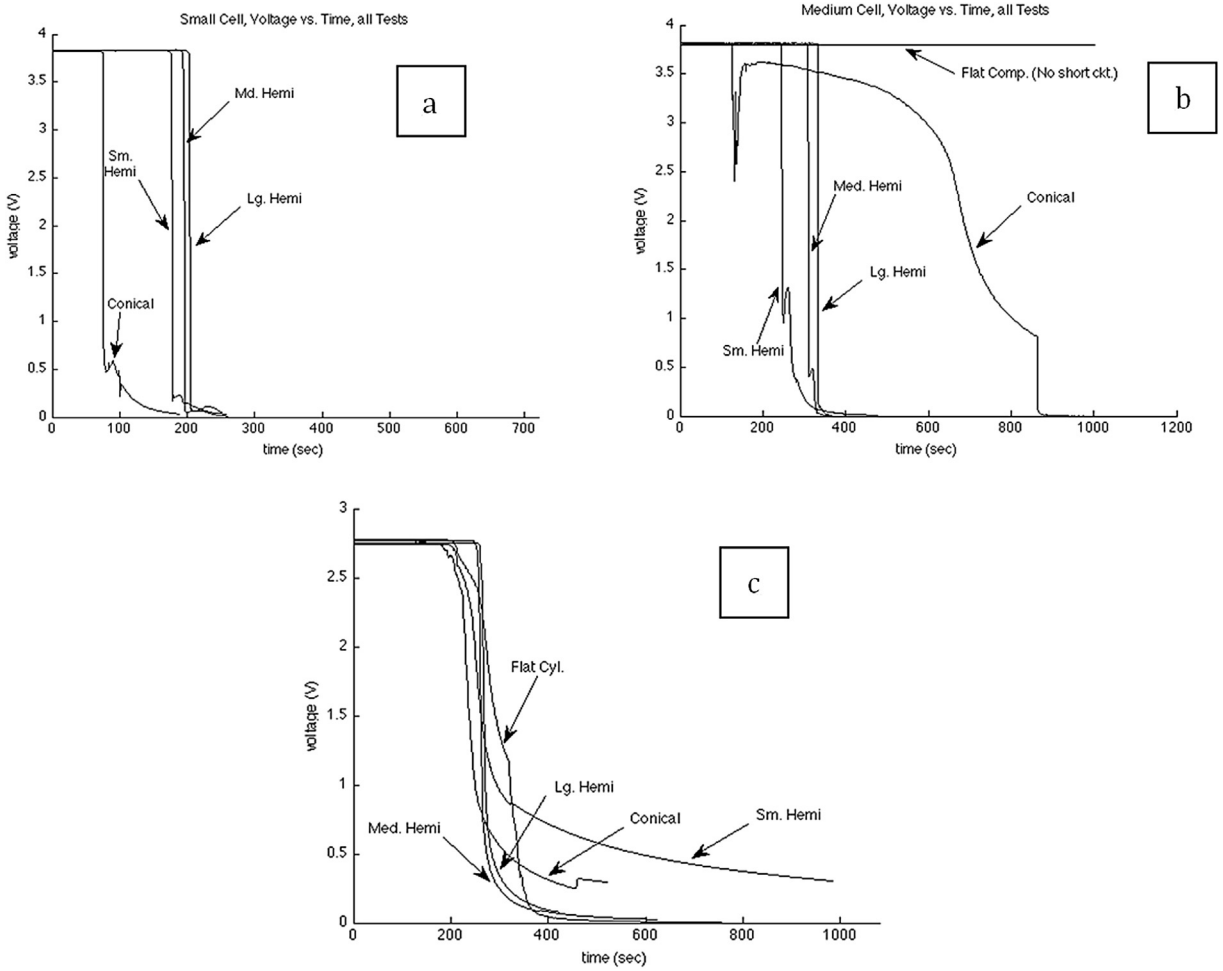

Fig. 7. The drop in voltage for a) small, b) medium, and c) large pouch cells.

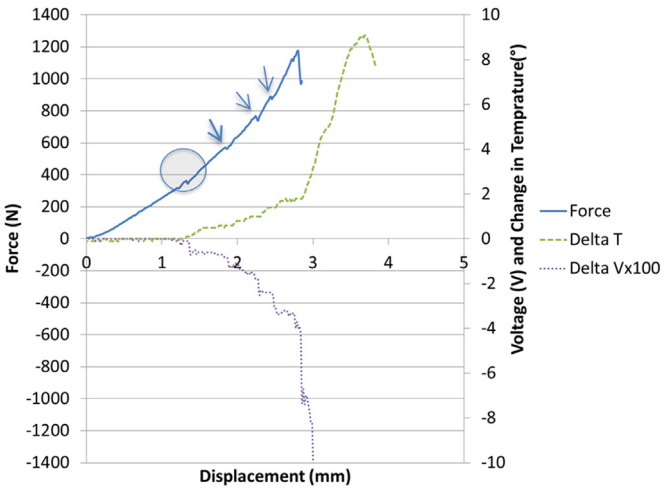

Fig. 8. Peak load (left) and deformation depth (right) at short circuit versus the diameter of the punch.

$$\sigma = 27.3\varepsilon \quad \text{for } \varepsilon < 0.09 \quad \sigma = 1997\varepsilon^{2.78} \quad \text{for } \varepsilon > 0.09 \text{ MPa} \tag{12}$$

The calibration results for the three cells are summarized in Table 4. Corresponding results for an 18650 cylindrical cell are also included for comparison [15].

A comparison of the stress–strain curves corresponding to three sizes of batteries is shown in Fig. 12. It is clear that there is no generic constitutive equation of the jellyroll. The compressive stress–strain curve depends on the material composition of the cell, thickness of various components of the electrode/separator assembly, strength of the binder, as well as the battery architecture.

The tensile properties of the jellyrolls were not directly determined from physical testing. A hybrid experimental-numerical method was used. This required construction of a Finite Element (FE) model of the cell, and calibrating the tensile strength from the small punch test for matching the peak force value at onset of short circuit from the tests. Details of the models are explained in next section.

4. Finite element model

For each cell, a finite element model was developed using the LS Dyna 971 software. The cells were modeled using fully integrated solid elements. It was assumed that contribution of the cell pouch is negligible. Therefore, the pouch was not modeled for any of the cells. All the elements were 1 mm cubes, with the exception of the small cell elements, which had 0.48 mm sides in the through thickness direction. There were 15,000 elements in the small cell, 33,810 elements in the medium cell, and 254,240 elements in the large cell.

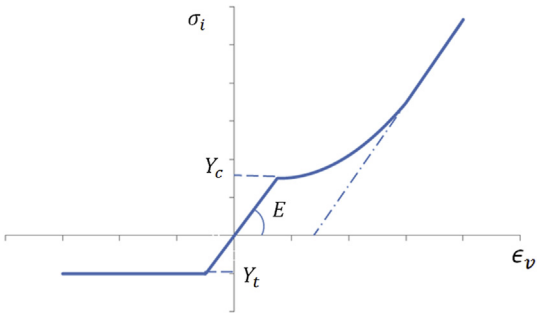

Fig. 10. The uniaxial representation of the assumed constitutive behavior.

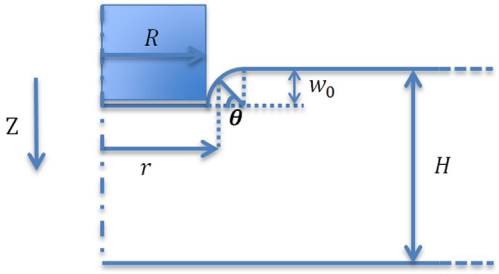

Fig. 11. Cross section of the large pouch cell, area under the flat circular punch, vertical dash line shows the axis of symmetry.

The lower surface of the cells rested on a rigid wall. The hemispherical punches were modeled using rigid shell elements. The material model crushable foam (Mat 63) is one of the simple, yet stable models in LS Dyna for modeling foams. The flow and hardening rules for this material are defined in principal stress space, and consistent with properties defined in previous section [21].

The stress–strain curves calibrated from the tests (see Table 4) were used as input for the volumetric strain hardening functions, $H(\varepsilon_v)$, to control compression properties of the cells. Initial yield (Y_c) was negligible for all the cells. As mentioned

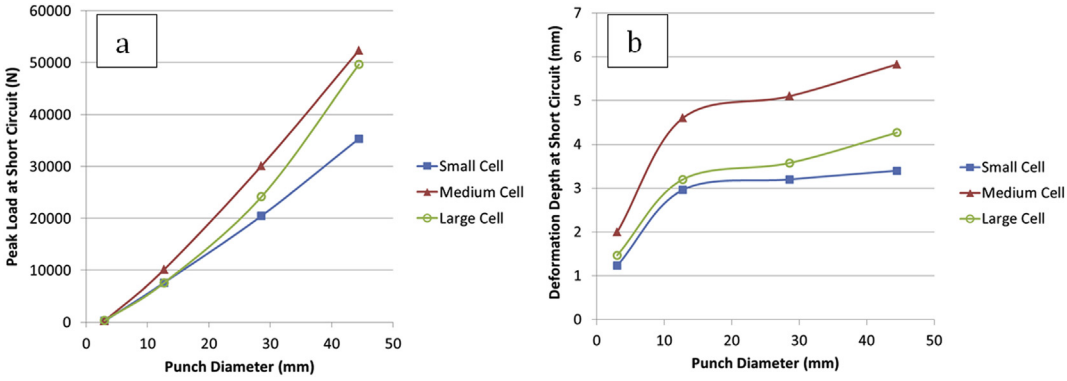

Fig. 9. Soft and hard internal short circuits for large cell, conical punch test.

Table 3
Contribution of the three terms in Equation (4).

$R = 12.655$ mm	$\int_0^R r dr$	$Rw_0 \int_0^{\frac{\pi}{2}} (1-\sin\theta)^{n+1}\sin\theta d\theta$	$w_0^2 \int_0^{\frac{\pi}{2}} (1-\sin\theta)^{n+1}\sin\theta(1-\cos\theta)d\theta$
$n = 1$	80.07	3.41	0.1125
$n = 2$	80.07	2.08	0.0432
$n = 3$	80.07	1.34	0.0198
$n = 4$	80.07	0.95	0.018

Table 4
Constitutive relation for the three types of cells.

Cell type	Compressive stress (*MPa*)	Tensile cut off (*MPa*)	Maximum principal strain (ϵ_f)
Small pouch	$\sigma = 426.3\epsilon^{1.7}$	$Y_t = 25$	0.14
Medium pouch	$\sigma = 276\epsilon^{1.8}$	$Y_t = 30$	0.16
Large pouch	$\sigma = 1997\epsilon^{2.78}$ for $\epsilon > 0.09$ and $\sigma = 27.3\epsilon$ for $\epsilon > 0.09$	$Y_t = 13$	0.11
Cylindrical [1]	$\sigma = 498\epsilon^2$	$Y_t = 10$	Not available

earlier, the small hemispherical punch tests were used to calibrate the tensile cut-off value, Y_t. The magnitude of Y_t was adjusted in the numerical simulation until the peak load corresponding to onset of short circuit in the test of small punch indentation for each cell is predicted at right point by the simulation. Element erosion was added to the material model by a maximum tensile strain criterion, ε_f, which again was calibrated from small punch indentation tests for each cell. Calibration values are reported in Table 4. A coefficient of friction of 0.25 was selected between the cell and the punch, as well as the cell and the flat rigid-wall underneath [22].

Fig. 13a shows the deformed meshes for the three cells, under small hemispherical punch loading. The load displacement curves for the simulations of small hemispherical punch of the three cells and the comparison to the corresponding tests are shown in Fig. 13b.

Fig. 13b shows that all three cell models closely follow the load displacement values observed during the tests. With the calibrated values of tensile cut off stress, and maximum principal strain, the drop in force which was verified as the point of short circuit in the tests, also matches closely between tests and simulations. The medium cell tolerates relatively larger loads and displacements before reaching short circuit. The small and large cells have similar peak loads at short circuit, although the large cell undergoes under slightly larger deformation before reaching short circuit.

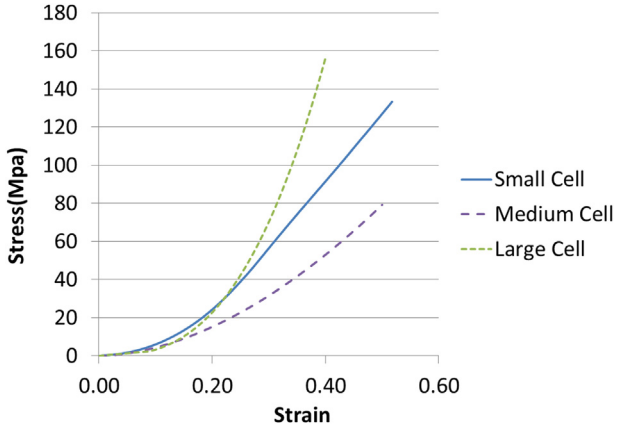

Fig. 12. Stress–Strain curves for the three pouch cells.

In the next step, the tests on small cells with medium and large hemispherical punches were simulated, see Fig. 14. The load displacement again was closely predicted; however, the peak load was slightly over predicted for large punch simulation. By reducing the coefficient of friction between large punch and the cell to 0.20, a closer prediction of the peak load corresponding to onset of short circuit was achieved. The peak force corresponding to short circuit for these punches increased to 20 and 35 kN, respectively.

For the conical punch simulation, original mesh size was too coarse to capture profile of deformation. Therefore, a new mesh of $0.2 \times 0.2 \times 0.4$ mm was developed in the center of the cell, where the punch contacts the cell surface. Fig. 15 shows the cross section of the revised mesh and the simulation of the conical punch indentation of the cell. Due to smaller size of elements the maximum principal strain at failure, ε_f, had to be recalibrated for this simulation.

Simulations of the medium and large hemispherical punch indentations into medium and large pouch cells were performed to further validate the proposed constitutive properties. Fig. 16 shows a comparison of each test and the corresponding simulation. For all of the four simulations, the original frictional coefficient of 0.25 was used without further trials to calibrate the coefficient. Despite slight difference in the peak load at short circuit, the capability of the model was very good both in determining the load-displacement relation, and the onset of short circuit.

5. Discussion and conclusions

An experimental compression and punch indentation program was completed on three types of pouch cells to understand their mechanical behavior under mechanical loading, and to investigate conditions leading to internal short circuit in the cells. It was observed during all punch indentation tests that short circuit occurred simultaneously with a local peak in force, a drop in voltage, and a rise in temperature. In a test of conical punch indentation into a large pouch cell, a soft short circuit preceded a complete short circuit; still the soft short was detectable in our carefully performed tests with same features: drops in force and voltage, and a rise in temperature. Although the magnitude of the changes in force, voltage, and temperature in the case of a soft short were significantly smaller than the complete short circuits observed in other cases, the peak force and deformation at soft

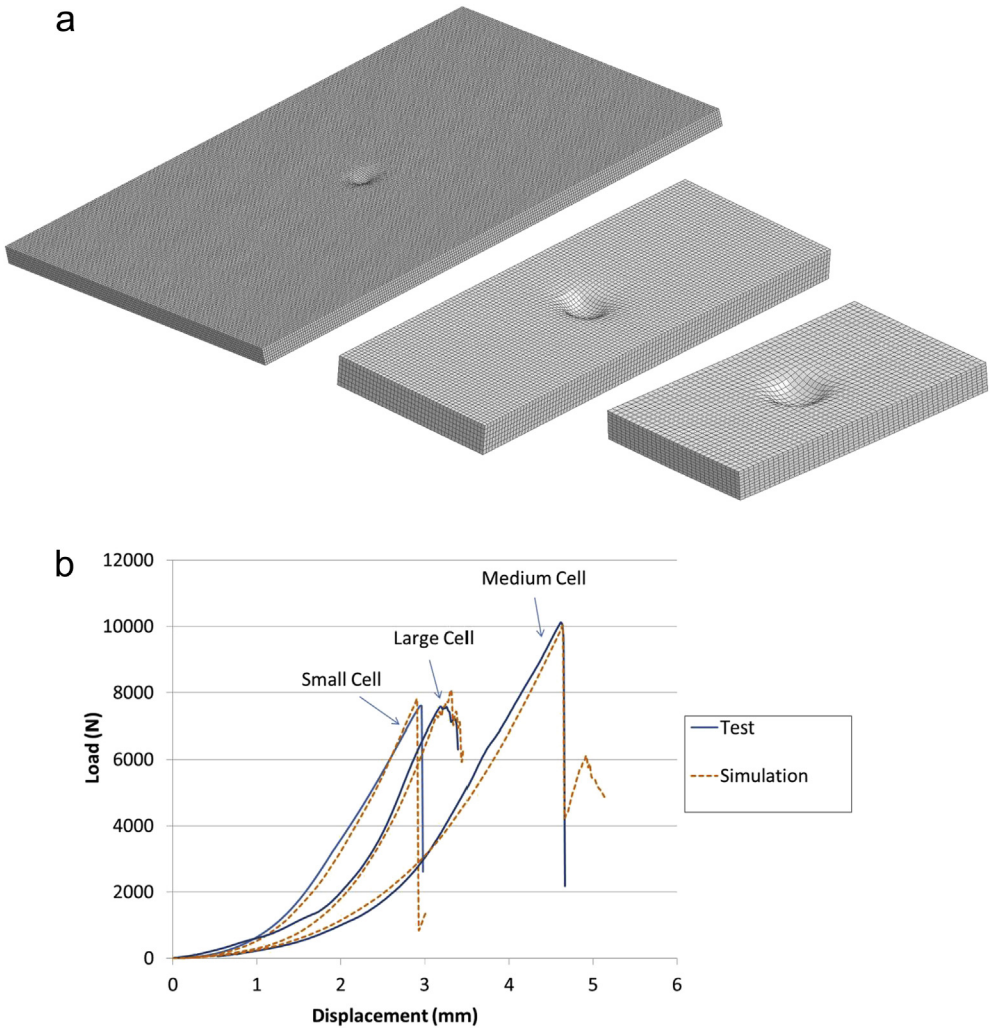

Fig. 13. a) Small hemispherical punch simulation for the three cells, b) Load-displacement curves, tests versus simulations for the small hemispherical punch test of the three cells.

short was within the expected values, based on the trends observed in all other cases. This is a significant finding, as it means from the extent of deformation alone, one can predict the possible existence of a soft short inside a cell, even if the voltage of the cell does not indicate an internal short circuit. It also means that manufacturing methods or applications that may cause a 1 mm dent in a pouch cell could introduce a soft short, leading to future catastrophic results without an immediately noticeable failure in the cell.

Results also showed a linear correlation between the radius of the indenter and the amount of force that it takes to create an interior short circuit in the cells. In the limiting case of a conical punch, a short circuit was created in the cells at deformations less than 2 mm, and loads less than 400 N, while a flat surface compression of the cell did not create a short circuit even at maximum apparatus load. Although somewhat intuitive, this information has important implications in the design of standards for crash/crush testing of battery cells and packs. It means a crush test that compresses a cell with a flat indenter may not address the issues that will be seen in real world when intrusion occurs asymmetrically and with narrower objects. For example, a side crash test of an automobile according to Federal Motor Vehicle Safety Standards (FMVSS 214) with a blunt, deformable barrier may not represent real word crash scenarios of electric vehicles, where longitudinal rails of the intruding vehicles could create more localized indentations.

In this research, a homogenized isotropic constitutive behavior for the jellyroll was proposed. It was shown that a hardening law in the form of $A\varepsilon^n$, with n in the range of 2–3, could model three types of pouch cells with different chemistries. Similar properties were observed for an 18650 cylindrical cell in prior research [15]. A new calibration method using a flat cylindrical punch was developed to calibrate cell parameters for large pouch cells. Compression between two flat plates, which works for small pouch cells, was not an option for large cells. Another parameter of the constitutive model is the tensile cut-off value. The magnitude of that parameter cannot be obtained from the compression tests, but can be obtained from local indentation tests, where tensile stresses develop beneath the punch.

A finite element model of each cell was then developed and the compressive properties were used to simulate the process of small punch indentation. From this simulation, a tensile cut off value was determined by matching the predicted and measured peak force to failure. The predicted load-displacement curves from the simulations were shown to closely replicate the curves recorded in the test program. Additionally, the local peak in force

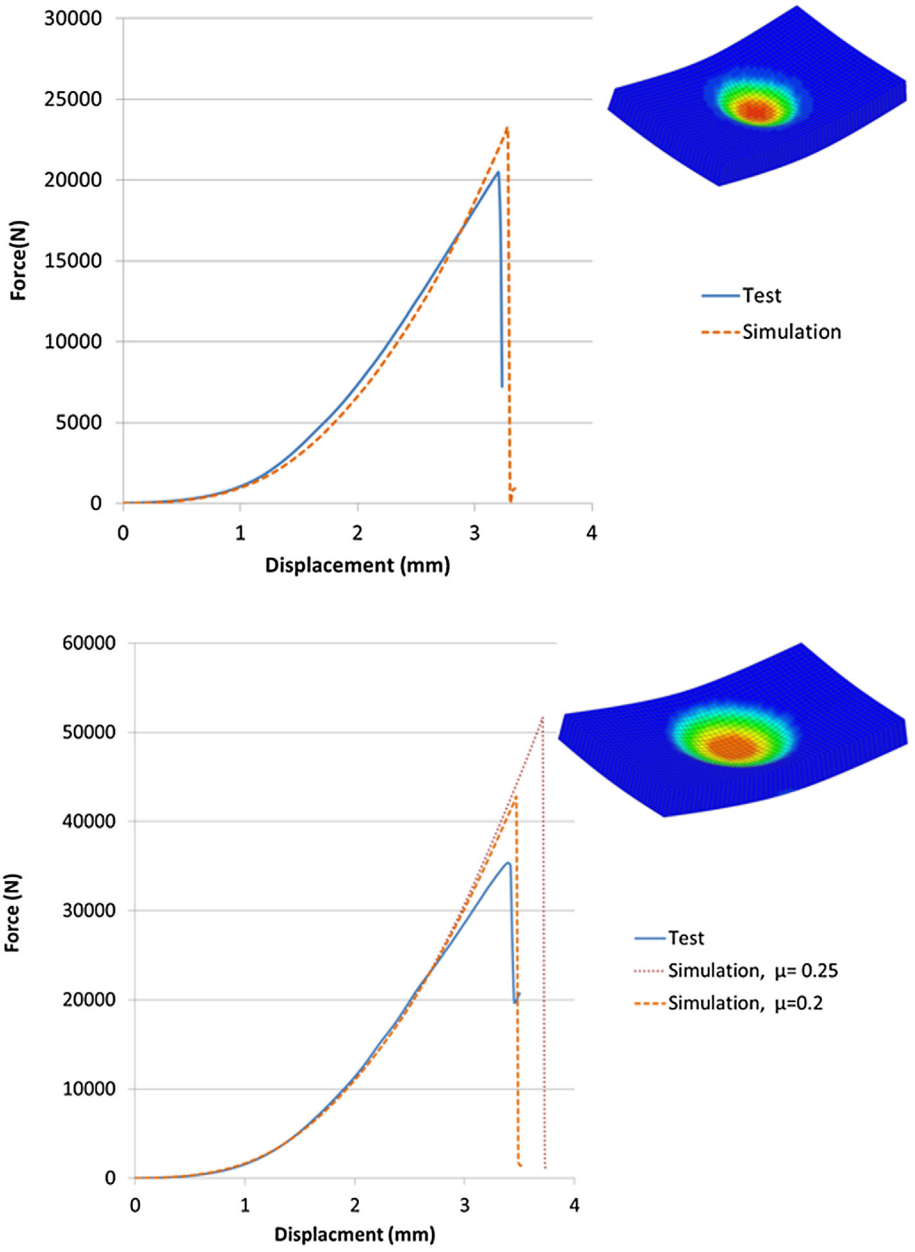

Fig. 14. Comparison of test and simulation for small pouch cell, top) medium hemispherical punch and bottom) large hemispherical punch.

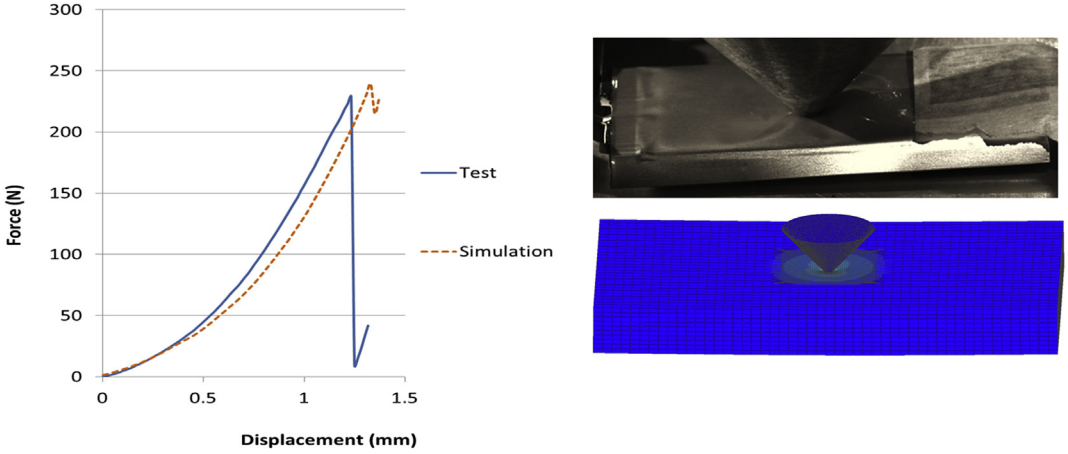

Fig. 15. Conical punch test and simulation, force-displacement left, figure of the test in top right, and cross section cut of simulation in bottom right.

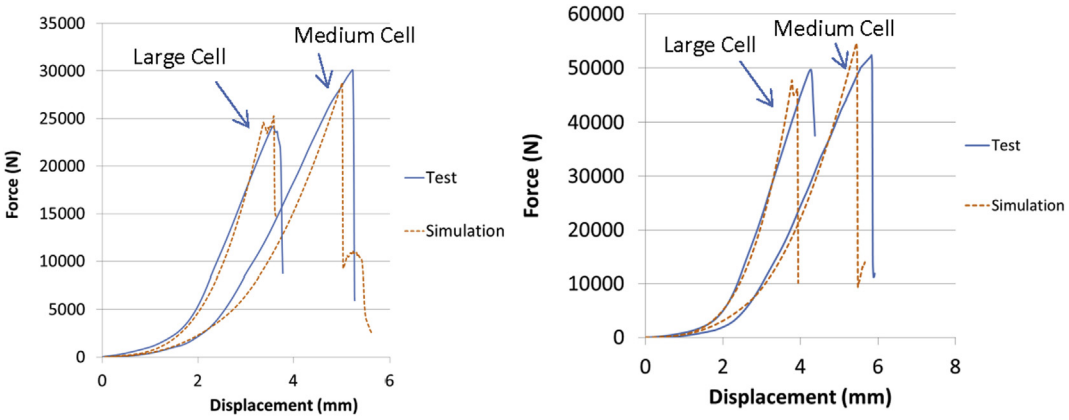

Fig. 16. Medium (left) and Large (right) hemispherical punch tests and simulations for medium and large pouch cells.

and the extent of deformation at the onset of short circuit were closely predicted.

The medium and large punch tests were also simulated with the same models for the purpose of validation. It was shown that the value of the coefficient of friction at the interface of the punch and cell is also important for exact prediction of the onset of short circuit. The friction can change from test to test and from one type of punch to the other. While an already good result can be obtained by keeping the friction coefficient constant and equal in all simulations, adjustment of the friction further refines the results.

Acknowledgments

Authors appreciate support of MIT Battery Consortium (Toyota and Volkswagen) as well as the Ford/MIT alliance for this research. Thanks are due to CDR John Campbell for performing the small pouch cell tests as part of his Master's thesis. Authors also acknowledge assistance of Altair Software for providing HyperWorks for this research.

Appendix A. Onset of short circuit for three types of pouch cells

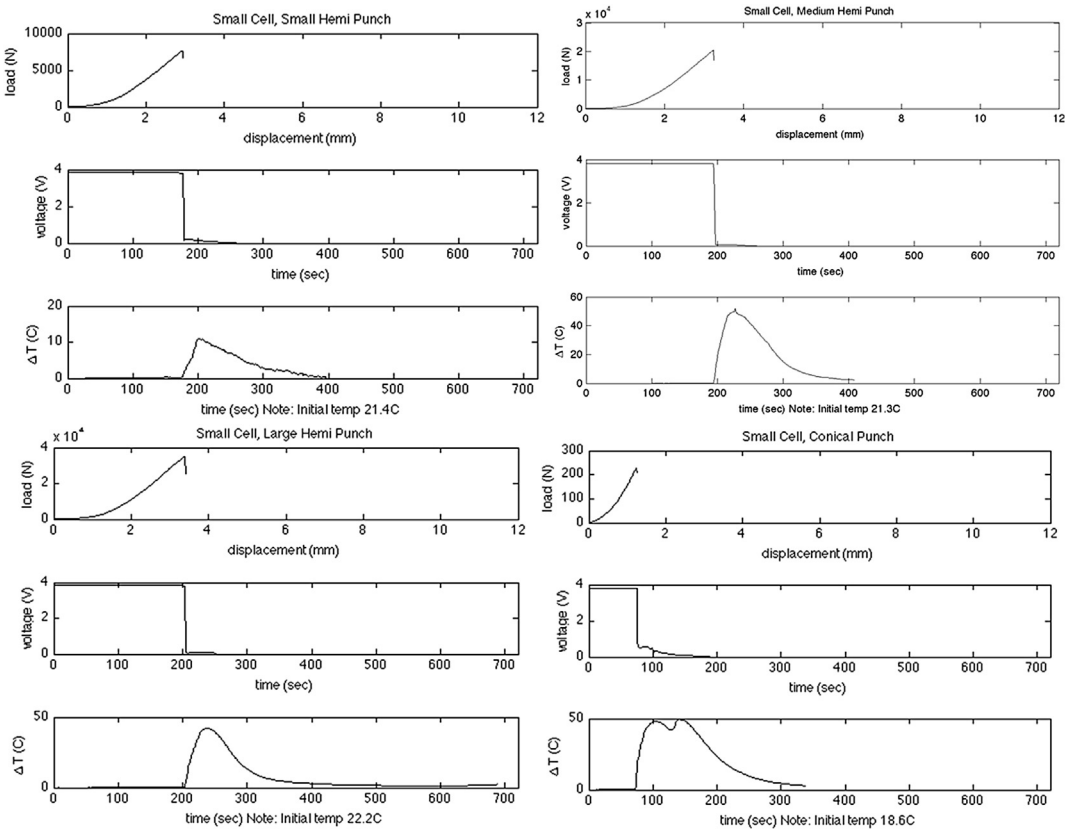

Fig. A 1. Results of hemispherical and conical punch tests on small pouch cells.

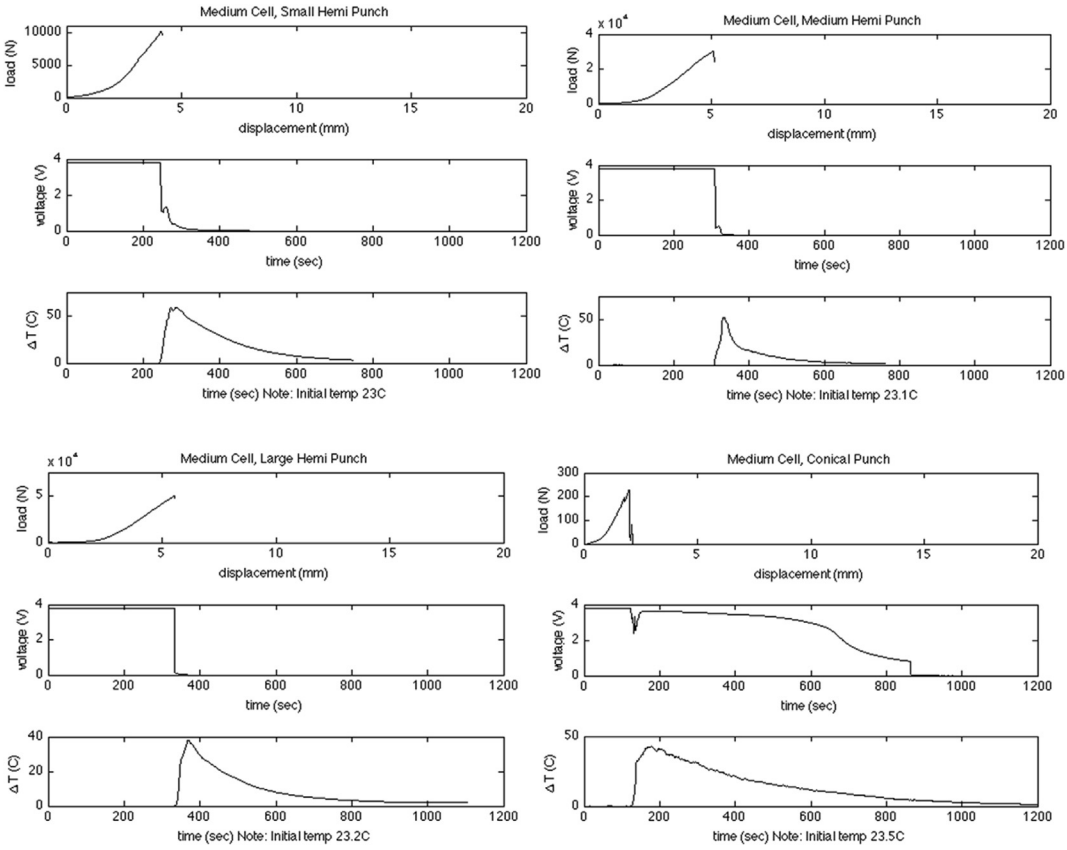

Fig. A 2. Results of hemispherical and conical punch tests on medium size cells.

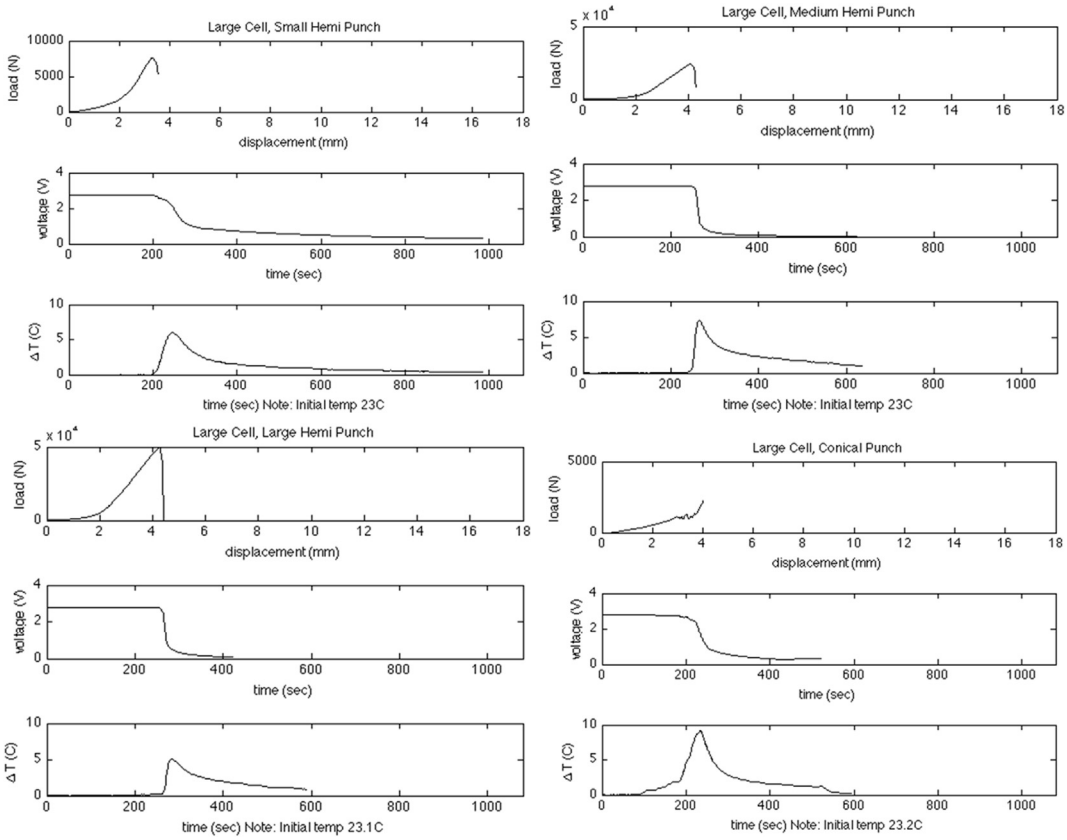

Fig. A 3. Results of hemispherical and conical punch tests on large size cells.

References

[1] J.O. Andy Pasztor. Business, Wall St. J. (2013) 1.
[2] B. Smith, DOT HS 811 573, 2012.
[3] W. Cai, H. Wang, H. Maleki, J. Howard, E. Lara-Cursio, J. Power Sources 196 (2011) 7779–7783.
[4] H. Maleki, J.N. Howard, J. Power Sources 191 (2009) 568–574.
[5] C.J. Orendorff, E.P. Roth, G. Nagasubramanian, J. Power Sources 196 (2011) 6554–6558.
[6] G. Kim, A. Pesaran, R. Spotnitz, J. Power Sources 170 (2007) 476–489.
[7] R. Spotnitz, J. Franklin, J. Power Sources 113 (2003) 81–100.
[8] R.M. Spotnitz, J. Weaver, G. Yeduvaka, D. Doughty, E. Roth, J. Power Sources 163 (2007) 1080–1086.
[9] D.H. Doughty, P.C. Butler, R.G. Jungst, E.P. Roth, J. Power Sources 110 (2002) 357–363.
[10] S. Golmon, K. Maute, M.L. Dunn, Comput. Struct. 87 (2009) 1567–1579.
[11] X. Zhang, W. Shyy, A.M. Sastry, J. Electrochem. Soc. 154 (2007) A910.
[12] X. Zhang, A.M. Sastry, W. Shyy, J. Electrochem. Soc. 155 (2008) A542.
[13] R. Fu, M. Xiao, S. Choe, J. Power Sources 224 (2012) 211–224.
[14] D. Shi, X. Xiao, X. Huang, H. Kia, J. Power Sources 196 (2011) 8129–8139.
[15] T. Wierzbicki, E. Sahraei, J. Power Sources (2013) 467–476.
[16] E. Sahraei, J. Campbell, T. Wierzbicki, J. Power Sources 220 (2012) 360–372.
[17] E. Sahraei, R. Hill, T. Wierzbicki, J. Power Sources 201 (2012) 307–321.
[18] L. Greve, C. Fehrenbach, J. Power Sources 214 (2012) 377–385.
[19] J. Meier, E. Sahraei, M. Salk, T. Kisters, F. Huberth, in: Proc. Battery Congress, 2013.
[20] B. Lawson, Battery and Energy Technologies: Why Batteries Fail. Available at:, 2013 (accessed 07.12) http://www.mpoweruk.com/failure_modes.htm.
[21] A. Hanssen, O. Hopperstad, M. Langseth, H. Ilstad, Int. J. Mech. Sci. 44 (2002) 359–406.
[22] J. Mens, A. De Gee, Wear 149 (1991) 255–268.